

# Low-Resource Quantum Energy Gap Estimation via Randomization

Hugo Pages,<sup>1,2,\*</sup> Chusei Kiumi,<sup>3</sup> Yuto Morohoshi,<sup>1</sup> Bálint Koczor,<sup>4</sup> and Kosuke Mitarai<sup>1,3</sup>

<sup>1</sup>*Graduate School of Engineering Science, The University of Osaka,  
1-3 Machikaneyama, Toyonaka, Osaka 560-8531, Japan.*

<sup>2</sup>*Télécom Physique Strasbourg, Strasbourg University,  
300 Bd Sébastien Brant, Illkirch Graffenstaden, 67412, France.*

<sup>3</sup>*Center for Quantum Information and Quantum Biology,*

*The University of Osaka, 1-2 Machikaneyama, Toyonaka, Osaka, 560-0043, Japan.*

<sup>4</sup>*Mathematical Institute, University of Oxford, Woodstock Road, Oxford OX2 6GG, United Kingdom.*

Estimating the energy spectra of quantum many-body systems is a fundamental task in quantum physics, with applications ranging from chemistry to condensed matter. Algorithmic shadow spectroscopy is a recent method that leverages randomized measurements on time-evolved quantum states to extract spectral information. However, implementing accurate time evolution with low-depth circuits remains a key challenge for near-term quantum hardware. In this work, we propose a hybrid quantum-classical protocol that integrates Time Evolution via Probabilistic Angle Interpolation (TE-PAI) into the shadow spectroscopy framework. TE-PAI enables the simulation of time evolution using shallow stochastic circuits while preserving unbiased estimates through quasiprobability sampling. We construct the combined estimator and derive its theoretical properties. Through numerical simulations, we demonstrate that our method accurately resolves energy gaps and exhibits enhanced robustness to gate noise compared to standard Trotter-based shadow spectroscopy. We further validate the protocol experimentally on up to 20 qubits using IBM quantum hardware. This makes TE-PAI shadow spectroscopy a promising tool for spectral analysis on noisy intermediate-scale quantum (NISQ) devices.

## I. INTRODUCTION

Quantum many-body systems are governed by the principles of quantum mechanics. A fundamental aspect of understanding these systems is the characterization of their energy spectra. In particular, the differences between eigenvalues of the Hamiltonian, often referred to as energy gaps, play an important role in determining their physical properties [1]. For instance, in quantum chemistry, excitation energies are directly related to molecular optical responses and chemical reactivity [2]. However, accurately computing energy gaps remains a challenging task for classical computers, primarily because the dimension of the Hilbert space that must be taken into account grows exponentially with the system size [3]. Quantum computers provide a promising alternative, as they are capable of simulating quantum systems efficiently with polynomially scaling resources with respect to the system size [4]—and indeed the earliest examples of quantum advantage are expected to be in quantum simulation [5, 6].

One of the earliest algorithms developed for estimating energy spectra on a quantum computer is quantum phase estimation (QPE) [7, 8]. It is often considered the main method within the framework of fault-tolerant quantum computing, as it can extract eigenvalues of a Hamiltonian with high precision. However, QPE requires deep circuits with ancillary qubits and error correction, which are far beyond the capabilities of current noisy intermediate-scale quantum (NISQ) devices. The limited

qubit counts, short coherence times, and high gate error rates in NISQ hardware make direct implementation of QPE infeasible in the near term, motivating the exploration of alternative approaches that are better suited to present-day hardware.

As such, researchers have proposed several quantum algorithms for estimating spectral properties, aiming for approaches that reduce circuit depth and resource requirements while remaining compatible with the constraints of current hardware. One promising method among them is algorithmic shadow spectroscopy [9]. In shadow spectroscopy, we apply the time evolution operator of a target Hamiltonian to qubits for various durations and perform randomized measurements at each time point to generate classical shadows. By collecting and analyzing these time-dependent signals, one can reconstruct spectral information through classical post-processing. A notable advantage of this method is that it requires only straightforward time evolution of the Hamiltonian without the need for ancilla qubits or controlled time evolution. Because of its simplicity, shadow spectroscopy offers better compatibility with near-term quantum devices compared to more demanding approaches such as quantum phase estimation [7, 8]. Also, by leveraging the classical shadow framework [10], it can estimate spectral properties with relatively few measurement shots, efficiently extracting relevant information from limited data. This feature provides a potential advantage over variational approaches such as the variational quantum eigensolver (VQE), which often require extensive optimization and large numbers of measurements to achieve comparable accuracy. However, this method still relies on precise time evolution, which can

\* [hugo.pages@etu.unistra.fr](mailto:hugo.pages@etu.unistra.fr)

make its implementation challenging depending on the capabilities of the quantum hardware. One approach to address this limitation is to apply quantum error mitigation techniques [11], such as probabilistic error cancellation, zero-noise extrapolation, or symmetry verification [12]. These approaches, however, require a detailed characterization of the noise and often lead to an exponential increase in the number of measurements.

To overcome this issue and further reduce the quantum resource requirements for spectral estimation, we propose an algorithm that integrates the recently developed technique of time-evolution via probabilistic angle interpolation (TE-PAI) into the framework of algorithmic shadow spectroscopy [13]. TE-PAI is a stochastic method for implementing time evolution under a given Hamiltonian based on Trotter decomposition. Instead of applying all gates in the Trotterized sequence, TE-PAI probabilistically samples a subset of rotation gates according to carefully chosen quasiprobability distributions [13–15]. This approach allows us to reproduce the effect of a long and accurate Trotter sequence using only a small number of quantum gates, significantly reducing circuit depth while preserving fidelity. Furthermore, TE-PAI requires only Pauli rotation gates with fixed angles of  $\Delta$  and  $\pi$ , followed by measurement. This approach, similar to shadow spectroscopy, does not rely on ancillary qubits or controlled time evolution. The simplicity and fundamental similarity of these randomized techniques make them naturally compatible and well aligned for integration. Although there is a trade-off between the measurement overhead and the number of gates, it is well understood and can be controlled explicitly [13]: Tuning the single parameter  $\Delta$  allows a user to increase or decrease the expected circuit depth at the cost of increasing the measurement overhead. Thus, the significant advantage of shadow spectroscopy—efficiently extracting spectral information with fewer shots—alleviates the increased shot requirement of TE-PAI.

By combining TE-PAI with algorithmic shadow spectroscopy, we construct an effective protocol for estimating energy spectra. Both TE-PAI and classical shadows involve sampling from randomized procedures, that is, one over gate sequences and the other over measurement bases. A key theoretical contribution of this work is the formulation of the combined estimator, which involves a nested quasiprobability sampling structure. This analysis ensures that the full protocol yields unbiased estimators of spectral quantities and clarifies the statistical properties of the resulting estimates.

Since our algorithm is theoretically shown to offer a significant reduction in quantum resource requirements, we further highlight its practicality through extensive numerical simulations, which form the main contribution of this work, and demonstrative experiments on existing quantum hardware. Thanks to the simplicity of its circuit construction, our algorithm has the potential to serve as a key enabler of practical quantum advantage for NISQ and early fault-tolerant quantum computers (early-

FTQC) [16].

While ref. [16] focused on the unique advantages of TE-PAI for early fault tolerant machines, we demonstrate a direct implementation of our algorithm on real quantum hardware through the simulation of the transverse Ising model. We benchmark its performance against conventional algorithmic shadow spectroscopy on a system of 20 qubits. Our results confirm the practical viability of our approach on contemporary noisy quantum devices, highlighting its potential for simulating many-body quantum systems within the current NISQ era.

This manuscript is organised as follows. Section II introduces the theoretical background. In Section III, we present the TE-PAI shadow spectroscopy protocol and provide a formal analysis of its unbiasedness and variance properties. Section IV reports numerical simulations and experimental results on quantum hardware, benchmarking the proposed method against standard Trotter-based shadow spectroscopy. Finally, Section V concludes with a discussion of the results, practical implications, and future research directions. Additional technical details and proofs are provided in the appendices.

## II. PRELIMINARIES

In this section, we introduce the necessary background for understanding our approach. Throughout this paper, we write boldface for quantum channels acting on density matrices. For a unitary  $U$ , the associated channel  $\mathbf{U}$  has the action  $\mathbf{U}(\rho) = U\rho U^\dagger$  for any density matrix  $\rho$ . For a  $d \times d$  matrix  $\rho = \sum_{i,j} \rho_{ij} |i\rangle\langle j|$ , we also introduce a vectorized notation as  $|\rho\rangle\langle\rho| := \sum_{i,j=1}^d \rho_{ij} |i\rangle\langle j|$ . With this convention, a channel corresponding to a unitary  $U$  can be written as  $|\mathbf{U}(\rho)\rangle\langle\rho| = (U^* \otimes U)|\rho\rangle\langle\rho|$ . We also introduce the Hilbert-Schmidt inner product between two operators  $A$  and  $B$  as  $\langle\langle A | B \rangle\rangle := \text{Tr}(A^\dagger B)$  in accordance with the Liouville space representation [17].

Our central goal is to enable the estimation of energy gaps from time-evolved classical shadow data using resource-efficient circuits optimized for the constraints of NISQ and early-FTQC quantum hardware.

### A. Energy Gap Estimation

Consider an  $N$ -qubit Hamiltonian  $H = \sum_{j=1}^J h_j P_j$ , where each  $P_j \in \{I, X, Y, Z\}^{\otimes N}$  is a Pauli string. The time evolution operator generated by  $H$  for a duration  $t$  is denoted by  $U_{H,t} := e^{-iHt}$ . Letting  $\{E_\alpha\}$  and  $\{|E_\alpha\rangle\}$  denote the eigenvalues and eigenstates of  $H$ , respectively, we define the energy gap between levels  $\alpha$  and  $\beta$  as:

$$\Delta E_{\alpha\beta} := |E_\alpha - E_\beta|.$$

The smallest nonzero energy gap is often simply called the energy gap, and it can govern important physi-

cal properties such as phase transitions, thermalization timescales, and adiabatic evolution rates.

In practice, quantum algorithms for gap estimation rely on extracting dynamical information from a time-evolved quantum state. Suppose a system with an initial state  $|\psi_{\text{init}}\rangle = \sum_{\alpha} c_{\alpha} |E_{\alpha}\rangle$  and evolves under  $H$  for time  $t$  as  $|\psi(t)\rangle = e^{-iHt} |\psi_{\text{init}}\rangle = \sum_{\alpha} c_{\alpha} e^{-iE_{\alpha}t} |E_{\alpha}\rangle$ . The expectation value of an observable  $O$  at time  $t$  becomes

$$\begin{aligned} S(t) &:= \langle \psi(t) | O | \psi(t) \rangle \\ &= \sum_{\alpha, \beta} c_{\alpha}^* c_{\beta} e^{i(E_{\alpha} - E_{\beta})t} \langle E_{\alpha} | O | E_{\beta} \rangle. \end{aligned} \quad (1)$$

The oscillatory terms in  $S(t)$  have frequencies equal to the energy differences  $\Delta E_{\alpha\beta}$ , and thus a Fourier transform of the time signal reveals peaks at these gaps.

Exact determination of  $\Delta E_{\alpha\beta}$  requires sufficiently precise and long time evolution to achieve the desired frequency resolution. On NISQ devices, however, implementing long and accurate time evolutions is challenging due to limited coherence times and gate imperfections.

## B. Time Evolution

From Eq. (1), efficiently simulating the time evolved state  $|\rho(t)\rangle := |U_{H,t}(\rho_{\text{init}})\rangle$  and estimating expectation values of many observables  $O$  denoted as

$$S(t) = \langle\langle O | \rho(t) \rangle\rangle$$

are key components of energy gap estimation algorithms in quantum computing. Since our target is NISQ and early-FTQC devices, we focus on methods that can implement time evolution with low quantum resource requirements.

One of the most straightforward approaches is Trotterization [4, 18, 19], which approximates  $U_{H,t}$  as a product of exponentials of individual terms in the Hamiltonian. Let  $K$  denote the number of Trotter steps and define the step size  $\delta t := t/K$ . The  $K$ -step Trotter circuit is denoted by  $U_{H,t}^{(K)}$  and is given by

$$U_{H,t}^{(K)} := \left[ \prod_{j=1}^J e^{-ih_j P_j \delta t} \right]^K = \left[ \prod_{j=1}^J R_{P_j, \theta_j} \right]^K, \quad (2)$$

where  $\theta_j = 2h_j \delta t$  and  $R_{P,\theta} := \exp(-i\theta P/2)$  is a Pauli rotation gate. The expectation value obtained by evolving  $\rho_{\text{init}}$  with the  $K$ -step Trotter circuit  $\langle O \rangle_t^{(K)} := \langle O | U_{H,t}^{(K)}(\rho_{\text{init}}) \rangle$  approximates the true expectation value as  $\epsilon_T := |S(t) - \langle O \rangle_t^{(K)}| \leq \mathcal{O}(t^2/K)$ . Also, the sample complexity scaling as  $\mathcal{O}(\epsilon_s^{-2})$  is required to estimate  $\langle O \rangle_t^{(K)}$  within an additive statistical error  $\epsilon_s$ .

We can further reduce the circuit depth required for time evolution by employing the recently proposed

method of time evolution via probabilistic angle interpolation (TE-PAI) [13, 14]. This method is based on quasiprobability sampling [20, 21] which we summarize in Section B.

For any  $\theta \in [0, \pi)$  and a fixed angle  $\Delta \in [|\theta|, \pi)$ , set  $\phi = \text{sign}(\theta)\Delta$ . A super operator representation of Pauli rotation  $R_{P,\theta} = \exp(-i\theta P/2)$  admits the decomposition

$$\mathbf{R}_{P,\theta} = a_1(\theta) \mathbf{R}_{P,1} + a_2(\theta) \mathbf{R}_{P,2} + a_3(\theta) \mathbf{R}_{P,3}, \quad (3)$$

where  $\mathbf{R}_{P,1}, \mathbf{R}_{P,2}, \mathbf{R}_{P,3}$  are super operator representations of Pauli rotation gates  $I, R_{P,\phi}, R_{P,\pi}$  and the coefficients are given as Eq. (C1). Let  $\gamma(\theta) := |a_1(\theta)| + |a_2(\theta)| + |a_3(\theta)|$  be the normalization factor. We define the random rotation channel outputting one of these three channels as  $\mathbf{R}_{P,l}$ , where  $l \in \{1, 2, 3\}$  is sampled with probabilities  $p_l(\theta) := |a_l(\theta)|/\gamma(\theta)$ . Fixing  $\Delta$  and applying the random-rotation construction independently to each Pauli-rotation gate  $R_{P_j, \theta_j}$  in the circuit  $U_{H,t}^{(K)}$  in Eq. (2), yields a random TE-PAI circuit

$$\hat{U}_{l,t}^{(K)} := \prod_{k=1}^K \prod_{j=1}^J \mathbf{R}_{P,l(j,k)}, \quad (4)$$

along with an accumulated classical weight  $\Gamma_l := \Gamma \prod_{k=1}^K \prod_{j=1}^J \text{sign}(a_{l(j,k)})$ , where  $\Gamma := \left( \prod_{j=1}^J \gamma(\theta_j) \right)^K$ . Here,  $l(j, k) \in \{1, 2, 3\}$  is sampled independently according to probability  $p_l(\theta_j)$  and by definition,  $\Gamma_l^2 = \Gamma^2$ .

Let  $\hat{o}_l$  be a single-shot measurement estimator of the observable  $O$  obtained by executing  $\hat{U}_{l,t}^{(K)}$  on  $\rho_{\text{init}}$ . The multiplication of  $\Gamma_l$  in post-processing yields an unbiased estimator of the original Trotter expectation value:

$$\mathbb{E}[\Gamma_l \hat{o}_l] = \langle O \rangle_t^{(K)} \approx S(t), \quad (5)$$

which approximates the true expectation value for sufficiently large  $K$ .

In implementation, each gate  $R_{P_j, \theta_j}$  is replaced by one of  $\{I, R_{P_j, \phi}, R_{P_j, \pi}\}$  and sampling  $I$  corresponds to skipping the gate. As  $K$  increases, the rotation angle  $\theta_j$  appearing in each Pauli rotation becomes smaller and the probability of skipping the gate approaches one, leading to a significant reduction of gates. As a consequence, the expected number of gates scales as  $\mathcal{O}(t)$  and converges to constant as  $K \rightarrow \infty$  whereas the number of gates in the Trotter circuit scales as  $\mathcal{O}(t^2)$  and diverges as  $K \rightarrow \infty$ . This reduction comes at the cost of a statistical sampling overhead, quantified by the accumulated weight  $\Gamma$ , which leads to a sample complexity scaling of  $\mathcal{O}(\Gamma^2 \epsilon_s^{-2})$ . Although this overhead factor  $\Gamma^2$  exhibits exponential scaling with the evolution time  $t$ , it converges to a constant in the limit of large  $K$  and the parameter  $\Delta$  enables a configurable trade-off between circuit depth and statistical sampling cost, ensuring the overhead remains manageable. A more detailed explanation of TE-PAI is provided in Section C.

### C. Shadow Spectroscopy

While the sampling overhead of TE-PAI is manageable, it becomes a critical bottleneck when scaling to a large number of observables. To circumvent this, we integrate the classical shadow framework [10]; by employing randomized measurements, this approach allows us to estimate exponentially many observables simultaneously with only logarithmic sample scaling. In particular, we utilize the Pauli-basis variant, which is well-suited for near-term hardware and enables the efficient reconstruction of local Pauli observables.

Given a quantum state  $\rho$ , we apply single-qubit Clifford unitaries  $U_1, \dots, U_N$  independently and uniformly at random, then measure in the computational basis to obtain a bitstring  $b = b_1 \dots b_N$ . From this outcome we construct a snapshot

$$|\hat{\rho}\rangle\rangle = \bigotimes_{n=1}^N (3U_n^{-1}|b_n\rangle\rangle - |I\rangle\rangle). \quad (6)$$

It follows that  $\mathbb{E}[|\hat{\rho}\rangle\rangle] = |\rho\rangle\rangle$ , so for any observable  $O$  the quantity  $\langle\langle O|\hat{\rho}\rangle\rangle$  is an unbiased estimator of  $\text{Tr}(O\rho)$ . By repeating the procedure many times, one obtains snapshots that allow simultaneous estimation of a large set of observables with rigorous sample complexity guarantees [10]. The key notion for analyzing the sample complexity is the shadow norm, which quantifies the variance of the estimator for a given observable. We define the squared shadow norm  $\|O\|_{\text{sh}}^2$  as the maximum second moment of the estimator over all possible states:

$$\|O\|_{\text{sh}}^2 := \max_{\rho} \mathbb{E} \left[ \langle\langle O|\hat{\rho}\rangle\rangle^2 \right], \quad (7)$$

where the expectation  $\mathbb{E}$  is taken over the random unitary transformations and measurement outcomes inherent to the shadow protocol. For the specific case of Pauli-basis measurements and observables that are  $q$ -local Pauli strings, the squared shadow norm is given as  $3^q$ . Then the overall sample complexity to estimate  $N_o$  observables within an additive error  $\epsilon$  is given as

$$\mathcal{O} [3^q \epsilon^{-2} \log(N_o)].$$

Finally, we employ the framework of algorithmic shadow spectroscopy [9]. We consider a sequence of time points  $\{t_n\}_{n=1}^{N_t}$ . Using the classical shadow snapshots  $\{\hat{\rho}(t_n)\}$  given by Eq. (6) from the state  $\rho(t_n)$  at each instance and a set of target observables  $\{O_i\}_{i=1}^{N_o}$ , we construct the estimated time series  $\hat{S}_i(t_n) = \langle\langle O_i|\hat{\rho}(t_n)\rangle\rangle$ . This procedure yields a total of  $N_o N_t$  data points while requiring a sample complexity of only  $\mathcal{O}(3^q N_t \epsilon^{-2} \log N_o)$  to estimate all  $N_o$  series simultaneously. Following standardization and statistical filtering, we compute the cross-correlations of these signals and perform a Fourier transform; the resulting spectral peaks reveal the energy gaps of the Hamiltonian. A detailed description of the process is provided in Appendix D.

### III. TE-PAI SHADOW SPECTROSCOPY

The central contribution of this work is a resource-efficient algorithm that integrates TE-PAI with algorithmic shadow spectroscopy. Explicitly designed for current and near-future quantum hardware, our protocol features a highly configurable trade-off between circuit depth and sampling overhead, minimizing quantum resource requirements while maintaining the flexibility to adapt to specific hardware constraints.

#### A. Our protocol

The following is the overview of the full procedure of TE-PAI shadow spectroscopy:

- Step 1: Generate TE-PAI Circuits.** Set the total Trotter steps as  $K_{\text{step}} = K \times N_t$  with positive integer  $K$  and the number of time points  $N_t$ , and decompose the time evolution operator  $e^{-iHt}$  into Trotter circuit  $U_{H,t_s}^{(sK)}$  for each time point  $t_s = s \frac{t}{N_t}$ . For each gate in the sequence, probabilistically replace it with a fixed-angle rotation  $\{0, \Delta, \pi\}$  to generate  $M_{\text{TE-PAI}}$  TE-PAI circuits along with classical weights  $(\Gamma_{t_m,t_s}, \hat{U}_{t_m,t_s}^{(sK)})$  according to Eq. (4).
- Step 2: Obtaining Shadow Snapshots.** Apply random single-qubit Clifford unitaries  $\{U_n\}_{n=1}^N$  to the state  $\hat{U}_{t_m,t_s}^{(sK)}(\rho_{\text{init}})$ , then measure in the computational basis to obtain a bitstring  $b = b_1 \dots b_N$ . We then classically store the snapshot as  $(\Gamma_{t_m,t_s}, \{U_n\}_{n=1}^N, \{b_n\}_{n=1}^N)$ .
- Step 3: Classical Signal Processing.** For  $N_o$  observables  $\{O_i\}_{i=1}^{N_o}$ , compute estimates of time series signals  $S_i(s) = \langle\langle O_i|\rho(t_s)\rangle\rangle$  from estimator  $\Gamma_{t_m,t_s} \langle\langle O_i|\hat{\rho}_{t_m}(t_s)\rangle\rangle$  which is constructed from the stored data according to Eq. (6). These time series are then processed, as described in Appendix D to extract the energy spectrum of the Hamiltonian.

The detailed pseudocode for Step 1 and Step 2 is provided in Algorithm 1. In our actual implementation, the process for generating these snapshots slightly differs from a simple repetition of the fundamental algorithm described in Algorithm 1. Specifically, our implementation generates one time-evolution circuit via the TE-PAI process and reuses it with  $N_s$  different randomized measurement bases to obtain  $N_s$  snapshots for each TE-PAI sampled circuits. Consequently, if we generate  $M_{\text{TE-PAI}}$  distinct time-evolution circuits via TE-PAI sampling, the total number of unique quantum circuits ultimately executed is  $M_{\text{TE-PAI}} \times N_s$ . The detailed pseudocode for this implementation is provided in Appendix E as Algorithm 2.

This modification allows us to control the total number of circuit executions directly, while independently varying  $M_{\text{TE-PAI}}$  and  $N_s$ . We show in the next subsection

---

**Algorithm 1** Obtaining a shadow snapshot of  $e^{-iHt}\rho_{\text{init}}e^{iHt}$  using TE-PAI

---

**Input:**  $N$ -qubit Hamiltonian  $H = \sum_{j=1}^J h_j P_j$ , initial state  $\rho_{\text{init}}$ , total time  $t$ , number of time steps  $K_{\text{steps}}$ , angle  $\Delta$

**Output:** Tuple  $(\Gamma, \{U_n\}_{n=1}^N, \{b_n\}_{n=1}^N)$ , where  $\Gamma \in \mathbb{R}$  is the post-processing weight,  $U_n$  is the local Clifford gate applied to qubit  $n$ , and  $b_n \in \{0, 1\}$ . The shadow is constructed as  $\Gamma \bigotimes_{n=1}^N [3U_n^{-1}|b_n\rangle\langle b_n| - |I\rangle\langle I|]$ .

- 1: Set  $\delta = t/K_{\text{steps}}$
- 2: Initialize  $\Gamma \leftarrow 1$
- 3: Initialize an empty quantum circuit  $\mathcal{C}$
- 4: **for**  $k = 1$  to  $K_{\text{steps}}$  **do**
- 5:   **for**  $j = 1$  to  $J$  **do**
- 6:     Compute  $\theta = -h_j \delta$
- 7:     Compute  $a_1, a_2, a_3$  according to Eq. (3)
- 8:     Set  $\gamma = |a_1| + |a_2| + |a_3|$ , sample  $d \in \{1, 2, 3\}$  with probability  $|a_d|/\gamma$
- 9:     Update  $\Gamma \leftarrow \Gamma \times \gamma \times \text{sign}(a_d)$
- 10:    Append gate  $R_{P_j, \phi}$  ( $\phi = \text{sign}(\theta)\Delta$  if  $d = 2$  or  $R_{P_j, \pi}$  if  $d = 3$ ) to  $\mathcal{C}$ ; if  $d = 1$ , append nothing
- 11:   **end for**
- 12: **end for**
- 13: **for**  $n = 1$  to  $N$  **do**
- 14:   Sample a Clifford gate  $U_n$  uniformly at random and add to qubit  $n$
- 15: **end for**
- 16: Apply  $\mathcal{C}$  to  $\rho_{\text{init}}$ , measure in the computational basis to obtain  $b = (b_1, \dots, b_N)$
- 17: **return**  $\Gamma, \{U_n\}, \{b_n\}$

---

that this modified implementation preserves the unbiased nature of the estimator.

## B. Formal Analysis

In this subsection, we analyze the statistical properties of the estimator obtained from TE-PAI shadow spectroscopy. For generality, we state the result not only for TE-PAI but can be applied to any quasiprobability sampling method.

We use the notation from Section B, where we consider a sequence of channels  $\mathbf{C} = \mathbf{C}_K \cdots \mathbf{C}_1$  with each  $\mathbf{C}_k$  decomposed as  $\mathbf{C}_k = \sum_{d=1}^D a_{k,d} \mathbf{C}_{k,d}$ . Let  $l_k \in \{1, \dots, D\}$  be a random variable drawn according to  $p_d = |a_{k,d}|/\gamma(\mathbf{C}_k)$ , where  $\gamma(\mathbf{C}_k) = \sum_d |a_{k,d}|$ . Define the random channel  $\hat{\mathbf{C}}_l := \mathbf{C}_{K,l_K} \cdots \mathbf{C}_{2,l_2} \mathbf{C}_{1,l_1}$  along with an accumulated classical weight  $\Gamma_l := \Gamma \prod_{k=1}^K \text{sign}(a_{k,l_k})$ , where  $\Gamma := \prod_{k=1}^K \gamma(\mathbf{C}_k)$ . We generate  $M$  independent samples of classical weight and circuit denoted as  $\Gamma_{l_m}, \hat{\mathbf{C}}_{l_m}$  with  $m \in \{1, \dots, M\}$ . For each sampled channel applied on the initial state  $\rho$ , we obtain  $N_s$  independent classical shadow snapshots  $\hat{\rho}_{m,s}$  ( $s \in \{1, \dots, N_s\}$ ) according to Eq. (6). We define the estimator  $o_{m,s} := \Gamma_{l_m} \langle\langle O | \hat{\rho}_{m,s} \rangle\rangle$

and the overall estimator as

$$\langle\hat{O}\rangle := \frac{1}{MN_s} \sum_{m=1}^M \sum_{s=1}^{N_s} o_{m,s}. \quad (8)$$

Then, the following theorem shows that the estimator  $\langle\hat{O}\rangle$  is an unbiased estimator of the true expectation value  $\langle\langle O | \mathbf{C}(\rho) \rangle\rangle$ . For specific case of TE-PAI,  $\mathbf{C}$  corresponds to the Trotterized time evolution channel  $\mathbf{U}_{H,t}^{(K)}$  and the true expectation value is  $\langle O \rangle_t^{(K)}$ .

**Theorem 1** (Unbiasedness). *The estimator defined in Eq. (8) is an unbiased estimator of the true expectation value:*

$$\mathbb{E}[\langle\hat{O}\rangle] = \langle\langle O | \mathbf{C}(\rho) \rangle\rangle,$$

where the expectation  $\mathbb{E}[\cdot]$  is taken over both the quasiprobability sampling and the randomized measurements for classical shadow.

The detailed proof is provided in Appendix E1. This demonstrates that the estimator remains unbiased regardless of  $M$  and  $N_s$ . The convergence to this true value is guaranteed by the law of large numbers.

The variance of the estimator is dominated by the statistical fluctuations inherent in the quasiprobability sampling. Increasing  $N_s$  reduces the variance from the shadow measurements for a fixed evolution circuit, but it does not reduce the variance arising from the choice of different evolution circuits. The latter is suppressed only by increasing the number of quasiprobability samples,  $M$ . Therefore, by increasing  $M$ , the estimator is guaranteed to converge to the true expectation value.

**Theorem 2** (Variance of the overall estimator). *The variance of this estimator is upper bounded as*

$$\text{Var}[\langle\hat{O}\rangle] \leq \Gamma^2 \left( \frac{\|O\|_{\text{sh}}^2 - \|O\|^2}{MN_s} + \frac{\|O\|^2}{M} \right).$$

For specific case of Pauli-basis measurements and normalized  $q$ -local Pauli observables, this becomes

$$\text{Var}[\langle\hat{O}\rangle] \leq \Gamma^2 \left( \frac{3^q - 1}{MN_s} + \frac{1}{M} \right).$$

The detailed proof is provided in Appendix E2.

By fixing the total number of circuit executions  $N_{\text{total}} := MN_s$ , we can further simplify the variance bound as

$$\text{Var}[\langle\hat{O}\rangle] \leq \frac{\Gamma^2}{N_{\text{total}}} (3^q - 1 + N_s).$$

This bound reveals a favorable trade-off for experimental implementation: as long as the number of shots per circuit satisfies  $N_s \lesssim 3^q$ , the statistical penalty for reusing the same circuit instance is small. Consequently, we can reuse a single compiled TE-PAI circuit instance up to

$N_s \ll 3^q$  times with negligible impact on the overall estimation error. This allows for significant amortization of circuit compilation and loading costs without compromising statistical precision. We numerically verify this behavior in Section IV A, demonstrating that the resulting spectrum depends mainly on the total shot budget.

## IV. EXPERIMENTS

In this section, we validate the performance of our proposed TE-PAI shadow spectroscopy protocol through a series of experiments conducted numerically and on quantum devices. We benchmark our method against the standard algorithmic shadow spectroscopy, which utilizes Trotterized time evolution as presented in Ref. [9]. Hereafter, we refer to the spectra from the standard and our proposed methods as the “Trotter-based spectrum” and the “TE-PAI-based spectrum,” respectively.

### A. Classical simulations

In this subsection, we demonstrate the efficacy and robustness of TE-PAI shadow spectroscopy through classical simulations. We first conduct a noise-free simulation to validate that our protocol can accurately recover the energy gaps of a target Hamiltonian under ideal conditions. Subsequently, we introduce a depolarizing noise model to assess the protocol’s resilience to gate errors, a critical factor for practical applications on near-term devices. Through these simulations, performed on a Heisenberg model using the Qiskit Aer simulator, we compare the performance of our method against the conventional Trotter-based approach, highlighting the advantages of TE-PAI in noisy environments.

For the noise-free simulations, we consider a 10-qubit one-dimensional Heisenberg model. The Hamiltonian used in our experiments is

$$\mathcal{H} = \sum_{i=1}^{N-1} (J_x X_i X_{i+1} + J_y Y_i Y_{i+1} + J_z Z_i Z_{i+1}), \quad (9)$$

where  $X_i, Y_i, Z_i$  are the Pauli operators acting on the  $i$ -th qubit.  $J_x, J_y$  and  $J_z$  are the coupling strength. They are set to 1 in our simulation. To isolate a specific energy gap, the initial state is prepared as a superposition of the ground state and the 10th excited state. To validate the energy spectrum used in our noise-free simulations, we consider the specific scaling and finite-size effects of the 1D isotropic Heisenberg model [22]. In this model, the theoretical energy gap is  $\Delta E \approx 4.3595$ . This value is commented in Appendix F. The time evolution is simulated for  $N_t = 90$  time points with a step of  $dt = 0.11$ . For both the TE-PAI and Trotter-based methods, the underlying Trotter decomposition uses  $K_{\text{steps}} = 650$  steps, and for TE-PAI, we set  $\Delta = \pi/2^7$ . Although the simulation of the circuits is noise-free, i.e., free from gate or

decoherence errors, we incorporate the statistical noise inherent in quantum measurements by taking only a single shot from each executed circuit. To ensure a fair comparison, we fix the total number of circuit executions to 1000 at each time point. For the standard Trotter-based method, this corresponds to simply taking  $N_s = 1000$  shadow snapshots. For the TE-PAI method, we set  $M_{\text{TE-PAI}} \times N_s = 1000$  and explore configurations such as  $(M_{\text{TE-PAI}}, N_s) = (1000, 1), (500, 2)$ , and  $(250, 4)$ . At each time point, we collect classical shadow snapshots and feed them into the algorithmic shadow spectroscopy protocol. Within this post-processing, we estimate the expectation values of all 3-local Pauli operators from the snapshots and retain only the top 10% of the most significant signals, which are identified using a Ljung-Box test (see also Appendix D for detailed procedure). The Ljung-Box test and the retention of the top 10% most significant signals constitute heuristic components of the spectral post-processing, adopted in line with prior work. A detailed assessment of the sensitivity to these choices is beyond the scope of this work; however, within the parameter ranges explored here, we do not observe qualitative changes in the extracted spectral features when these thresholds are varied moderately.

Figure 1 shows the energy spectra obtained from the noise-free simulation. As can be seen, both the Trotter-based method (blue dotted line) and our TE-PAI-based approach (solid lines) successfully identify the theoretical energy gap at  $\Delta E \approx 4.36$ , which validates the fundamental principle and correctness of our protocol. A clear difference, however, appears in the signal intensity; for a fixed total number of 1000 circuit executions, the Trotter-based spectrum exhibits a significantly higher peak. This reduced intensity for the TE-PAI method is an expected consequence of the additional statistical variance introduced by the quasiprobability sampling of gates. As discussed in Ref. [13], this variance necessitates a larger number of total samples to achieve the same signal-to-noise ratio as the deterministic Trotter evolution. However, this higher sampling cost is the trade-off for the primary advantage of TE-PAI: a significant reduction in circuit depth, which provides crucial robustness against gate errors, as we will demonstrate later.

A second, notable finding from Fig. 1 is the internal consistency of the TE-PAI results. The peak intensity remains nearly identical regardless of how the 1000 total executions are distributed between the number of TE-PAI samples,  $M_{\text{TE-PAI}}$ , and the shadow snapshots per sample,  $N_s$ . This is a non-trivial observation, as it empirically validates that the statistical precision of our hybrid protocol is determined solely by the total number of samples, not the specific strategy used to obtain them. This finding has significant practical implications, as it offers the flexibility to choose the most convenient balance between generating many distinct evolution circuits (large  $M_{\text{TE-PAI}}$ ) and performing more measurements on fewer circuits (large  $N_s$ ) without affecting the final signal-to-noise ratio for a fixed total cost, see Appendix G for

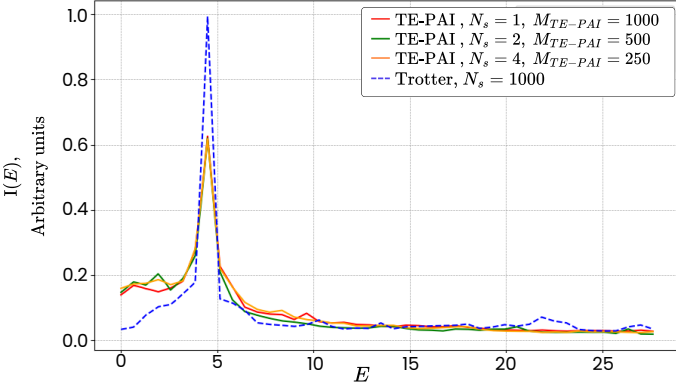


FIG. 1. Energy spectra of the 10-qubit Heisenberg model from our TE-PAI-based method (solid lines) and the Trotter-based method (dotted line), with the total number of circuit executions fixed at 1000. The legend details the combinations of TE-PAI samples ( $M_{TE-PAI}$ ) and shadow snapshots ( $N_s$ ). For the same execution cost, the Trotter-based method shows a higher peak intensity, while the TE-PAI results are consistent across different configurations.

simulation with Large  $N_s$ .

Next, to assess the protocol’s performance under more realistic conditions, we perform simulations on a 6-qubit Heisenberg model with a depolarizing noise model. First, we construct the quantum circuits with a gateset consisting of  $R_X, R_Z, R_{XX}, R_{YY}, R_{ZZ}$  Pauli rotations. We then introduce depolarizing noise after each gate, with an error probability of  $p_1 = 10^{-4}$  for single-qubit gates and  $p_2 = 10^{-3}$  for two-qubit gates. For this experiment, we set the number of Trotter steps to  $K_{\text{steps}} = 300$  and the total number of circuit executions to 3000. The PAI with  $\Delta = \pi/2^5$  is used to reduce circuit depth. In this setup, the Trotter-based circuits for  $K_{\text{steps}} = 300$  have an average depth of about 1810, while the corresponding TE-PAI circuits have an average depth of about 751. The depth is calculated as the minimum number of sequential layers of gates needed to execute the circuit, i.e., the length of the longest path through gates with qubits not sharing a layer. It was obtained in the simulation using Qiskit QuantumCircuit.depth method [23], version = "1.4.2".

Figure 2 shows the results of the noisy simulation, comparing them against the noise-free case. The outcome reveals a stark difference in noise robustness. The TE-PAI spectrum is only slightly degraded by the noise and the spectral peak remains clearly resolved. In contrast, the Trotter-based spectrum collapses, as the noise almost entirely suppresses the peak. This result confirms the superior noise resilience of the TE-PAI method, a direct consequence of its significantly shallower circuits.

## B. Experiments on quantum hardware

To demonstrate the practical viability of our protocol, we present experiments for a 20-qubit transverse-field

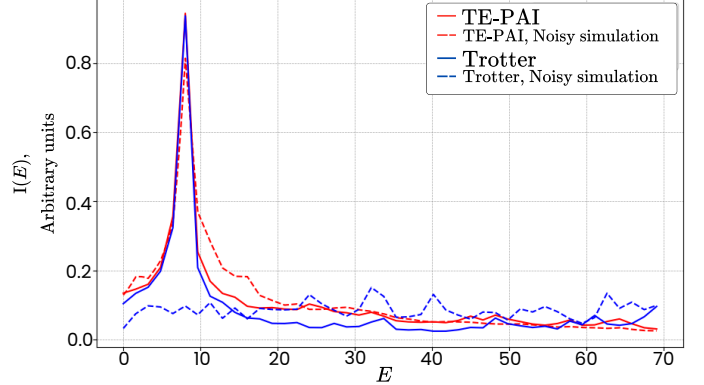


FIG. 2. Effect of depolarizing noise on the energy spectra obtained from TE-PAI (red) and Trotter-based (blue) methods. Dotted lines represent the noise-free benchmarks, while solid lines show the results under noise. The TE-PAI spectrum demonstrates strong robustness, with its peak remaining clearly visible. In contrast, the Trotter-based spectrum collapses, losing nearly all spectral information. This highlights the practical advantage of TE-PAI’s shallower circuits in noisy environments.

Ising model on IBM quantum hardware. The Hamiltonian for this model is

$$H = -J \sum_{k=1}^{N-1} Z_k Z_{k+1} - d \sum_{k=1}^N X_k. \quad (10)$$

The theoretical gap between the ground and first excited states is  $\Delta E = 2\sqrt{J^2 + d^2 - 2Jd \cos(\pi/(N+1))}$  [24]. As a practical compromise between preparation efficiency and sufficient overlap with these states, we use the initial state  $|+\cdots+0\rangle$  and set the parameters to  $J = 0.1$  and  $d = 2$ . We set the number of Trotter steps to  $K_{\text{steps}} = 115$  and use a TE-PAI angle of  $\Delta = \pi/2^5$ , which limits the average circuit depth to approximately 600. For the time evolution, we use  $N_t = 80$  steps with an interval of  $dt = 0.037$ . At each time point, we perform 3000 total circuit executions, configured as  $(M_{TE-PAI}, N_s) = (3000, 1)$ . From the resulting shadow snapshots, the algorithmic shadow spectroscopy process is performed in exactly the same manner as the classical simulation. We run these experiments on the *ibm\_kobe* and *ibm\_kingston* quantum computers, whose detailed properties are provided in Appendix H.

Figure 3 shows the spectra from our experiments on quantum hardware. The data from both the *ibm\_kobe* (red line) and *ibm\_kingston* (green line) devices correctly resolve the theoretical energy gap, confirming our protocol’s viability under realistic noise conditions. We observe a higher peak from *ibm\_kobe*, which is consistent with its lower average gate error rate as detailed in Appendix H. Crucially, the TE-PAI spectrum is more pronounced than the one from the conventional Trotter-based method (blue dotted line) run on the same device. This result provides direct experimental evidence that the shallower circuits produced by TE-PAI lead to

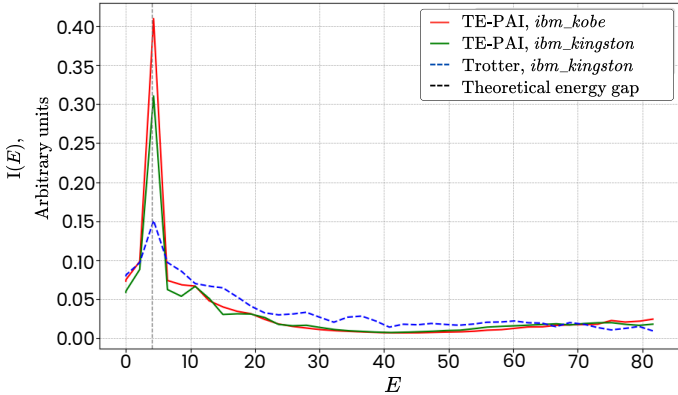


FIG. 3. Spectra of a 20-qubit Transverse Ising Hamiltonian measured on quantum hardware. The red and green line show a TE-PAI based spectrum performed respectively on *ibm\_kobe* and *ibm\_kingston*. The blue dotted line shows a Trotter based spectrum performed on *ibm\_kingston*. The grey dotted vertical line indicates the exact energy gap.

superior robustness against hardware noise. It thereby marks a significant scale-up from the 6-qubit hardware demonstration in the original work [9].

## V. CONCLUSION

In this work, we introduced TE-PAI shadow spectroscopy, a hybrid quantum-classical protocol that integrates the randomized time evolution of TE-PAI with the measurement framework of algorithmic shadow spectroscopy. We have theoretically established that this combination yields an unbiased estimator for spectral properties and experimentally validated its performance. Our noise-free classical simulations confirmed that the protocol correctly identifies energy gaps, while also highlighting an inherent trade-off: the quasiprobability sampling in TE-PAI introduces statistical variance that requires a larger number of total circuit executions to achieve the same signal intensity as the standard Trotter-based method. However, this cost is made up for by the protocol's primary advantage, which we demonstrated in noisy simulations: a significant reduction in circuit depth leads to superior robustness against gate errors. This key benefit was further confirmed through experiments on 20-qubit quantum hardware, where our method successfully resolved the target energy gap and outperformed the conventional approach, demonstrating its practical viability for spectroscopy in a significantly larger scale experiment than previously performed.

Let us briefly address the practical time complexity of our protocol compared to standard approaches. While TE-PAI utilizes  $M_{\text{TE-PAI}}$  unique circuit instances rather than a single reused circuit, the efficiency of modern control stacks prevents this from causing a significant increase in wall-clock execution time. Current quantum runtime environments (such as Qiskit Runtime) support

circuit batching, allowing the full ensemble of  $M_{\text{TE-PAI}}$  circuits to be submitted and executed within a single job, thereby avoiding the latency overhead associated with multiple job submissions. Furthermore, our variance analysis (Theorem 2) and numerical results (Fig. 1) demonstrate that the estimator remains unbiased even when reusing a single compiled circuit instance for  $N_s$  shots. This allows for the compilation and loading costs to be amortized over  $N_s$  measurements. By optimizing the ratio of unique circuits ( $M$ ) to shots-per-circuit ( $N_s$ ) for a fixed total budget, one can balance the statistical requirements against the hardware's specific compilation and loading latencies, rendering the total wall-clock time comparable to standard Trotterized evolution.

Looking forward, TE-PAI shadow spectroscopy opens several promising research avenues. The natural trade-off between circuit depth and sampling overhead constitutes a tunable design parameter that can be optimized in accordance with the specific performance characteristics of the underlying quantum hardware. In particular, quantum devices with lower error rates can reliably support deeper circuits, thereby reducing the required sampling overhead. Conversely, on hardware with higher error rates, circuit depth can be deliberately curtailed at the expense of increased sampling overhead, enabling a more favorable balance between noise resilience and statistical accuracy. A natural next step would be to combine our protocol with other error mitigation techniques, such as readout error correction or zero-noise extrapolation, to further suppress the impact of device imperfections. Furthermore, the demonstrated scalability and noise resilience make our method a strong candidate for tackling challenging problems in quantum chemistry and condensed matter physics, where deep circuits have been a major bottleneck. The flexibility in distributing the sampling budget between the number of TE-PAI circuits and shadow snapshots also suggests possibilities for hardware-aware co-design of experiments, potentially leading to even more efficient spectral analysis on near-term quantum computers.

**Data availability:** The simulation code used in this work is available online at : [https://github.com/hugopgs/TE-PAI\\_shadow\\_spectroscopy](https://github.com/hugopgs/TE-PAI_shadow_spectroscopy).

## ACKNOWLEDGMENTS

Y.M. is supported by JST SPRING under Grant Number JPMJSP2138. This work is partially supported by JST ASPIRE Japan Grant Number JPMJAP2319, the project JPNP20017 funded by the New Energy and Industrial Technology Development Organization (NEDO), JST COI-NEXT program Grant No. JPMJPF201. K.M. is supported by JST FOREST Grant No. JPMJFR232Z, JSPS KAKENHI Grant No. 23H03819, 24K16980 and JST CREST Grant No. JPMJCR24I4. C.K. is supported by JST PRESTO, Japan, Grant Number JP-MJPR25F1. This work, as part of the ITI 2021–2028

program of the University of Strasbourg, CNRS and Inserm, was supported by IdEx Unistra (ANR-10-IDEX-0002), and by SFRI STRAT'US project (ANR-20-SFRI-0012) and EUR QMAT ANR-17-EURE-0024 under the framework of the French Investments for the Future Program. B.K. thanks UKRI for the Future Leaders Fellowship Theory to Enable Practical Quantum Advantage (MR/Y015843/1) and EPSRC for funding through the project Software Enabling Early Quantum Advantage (SEEqA, EP/Y004655/1). This research was funded in part by UKRI (MR/Y015843/1). For the purpose of Open Access, the author has applied a CC BY public copyright licence to any Author Accepted Manuscript version arising from this submission.

## Appendix A: Product Formulas

Throughout this work, we employ the first-order Trotter product formula. The associated Trotter error, arising from the discretization of time evolution, is an intensively studied topic [25]; here, we briefly summarize the relevant results. Let  $U_{H,t}^{(K)}$  denote the Trotter circuit defined in Eq. (2) with  $K$  Trotter steps. The spectral norm error between the exact time evolution operator  $U_{H,t}$  and the approximation  $U_{H,t}^{(K)}$  is bounded by:

$$\left| U_{H,t} - U_{H,t}^{(K)} \right| \leq \frac{t^2 |c|_T}{2K},$$

where  $\|c\|_T := \sum_{\gamma < \beta} \| [h_\gamma P_\gamma, h_\beta P_\beta] \|$  is the commutator norm of  $H$ . The error in the estimated expectation value induced by the Trotter approximation is bounded by the operator error and the spectral norm of the observable:

$$\begin{aligned} \epsilon_T &:= \left| S(t) - \langle O \rangle_t^{(K)} \right| \\ &\leq 2\|O\| \left\| U_{H,t} - U_{H,t}^{(K)} \right\| \\ &\leq \frac{t^2 \|O\| \|c\|_T}{K}, \end{aligned}$$

where  $\langle O \rangle_t^{(K)} := \langle O | U_H^{(K)}(t)(\rho) \rangle$  denotes the expectation value obtained by evolving  $\rho$  with the  $K$ -step Trotter circuit. As  $K$  increases, the Trotter approximation converges to the exact evolution, so the Trotter error vanishes in the limit  $K \rightarrow \infty$  (the bound above scales as  $O(t^2/K)$ ); moreover, this is a worst-case upper bound, and the empirical error for specific instances is often much smaller [25].

Other than the Trotter error, finite sampling introduces statistical error. To estimate  $\langle O \rangle_t^{(K)}$  on hardware, we sample  $N$  independent measurement outcomes  $o_1, \dots, o_N$  from repeated executions of the Trotter circuit  $U_H^{(K)}(t)$  and use the sample mean  $\hat{o} := \frac{1}{N} \sum_{n=1}^N o_n$ . Then  $\mathbb{E}[\hat{o}] = \langle O \rangle_t^{(K)}$  and  $\text{Var}(\hat{o}) \leq \|O\|^2/N$ , leading to a

sample complexity scaling as

$$N = \mathcal{O}\left(\frac{\|O\|^2 \log(1/\delta)}{\epsilon^2}\right),$$

to achieve additive error  $\epsilon$  with failure probability  $\delta$ .

## Appendix B: Quasiprobability sampling

The theoretical results presented in Section III B are not limited to TE-PAI but apply generally to any quasiprobability sampling method. Here, we briefly review this underlying framework.

In this approach, quantum channels that are difficult to implement exactly are approximated by randomly sampling from a set of simpler operations. This strategy is mathematically grounded in quasi-probability decompositions, which serve as the foundation for many randomized compiling techniques. Prominent examples include probabilistic error cancellation (PEC) for stochastic noise mitigation [21, 26, 27], probabilistic angle interpolation (PAI) for coherent or synthesis-error mitigation [13, 14, 28], and circuit cutting [29–31].

Suppose a target channel  $\mathbf{C}$  can be decomposed as a linear combination

$$\mathbf{C} = \sum_{d=1}^D a_d \mathbf{C}_d,$$

where  $a_d \in \mathbb{R}$  are real coefficients and  $\{\mathbf{C}_d\}$  is a set of efficiently implementable basis channels. We define the normalization factor  $\gamma(\mathbf{C}) = \sum_{d=1}^D |a_d|$  and assign sampling probabilities  $p_d = |a_d|/\gamma(\mathbf{C})$ .

To simulate  $\mathbf{C}$ , we sample an index  $l \in \{1, \dots, D\}$  from the distribution  $\{p_l\}$ , apply the channel  $\mathbf{C}_l$ , and weight the measurement outcome by  $\gamma(\mathbf{C})\text{sign}(a_l)$ . This weighting is performed via classical post-processing; specifically, for any observable  $O$  and state  $\rho$ , the expectation value satisfies:

$$\langle O | \mathbf{C}(\rho) \rangle = \gamma(\mathbf{C}) \mathbb{E}[\text{sign}(a_l) \langle O | \mathbf{C}_l(\rho) \rangle],$$

where the expectation is taken over the random choice of  $l$ . Consequently, the resulting random estimator is unbiased, satisfying

$$\mathbb{E}[\gamma(\mathbf{C})\text{sign}(a_l)\mathbf{C}_l] = \mathbf{C}.$$

Next, we consider a sequential channel  $\mathbf{C} = \mathbf{C}_K \cdots \mathbf{C}_1$  with each  $\mathbf{C}_k$  decomposed as

$$\mathbf{C}_k = \sum_{d=1}^D a_{k,d} \mathbf{C}_{k,d}$$

where  $\mathbf{C}_{k,d}$  are efficiently implementable channels. Let  $l_k \in \{1, \dots, D\}$  be a random variable drawn according to

$p_d = |a_{k,d}|/\gamma(\mathbf{C}_k)$ , where  $\gamma(\mathbf{C}_k) = \sum_d |a_{k,d}|$ . Define the random channel

$$\hat{\mathbf{C}}_l := \mathbf{C}_{K,l_K} \cdots \mathbf{C}_{2,l_2} \mathbf{C}_{1,l_1}$$

with the classical post-processing weight  $\Gamma_l = \prod_{k=1}^K \gamma(\mathbf{C}_k) \text{sign}(a_{k,l_k})$ . For any initial state  $\rho$ , applying the sampled channel sequence produces an unbiased estimator of  $\mathbf{C}(\rho)$  as

$$\mathbb{E}[\Gamma_l \hat{\mathbf{C}}_l(\rho)] = \mathbf{C}(\rho).$$

While this re-weighting guarantees unbiasedness, it scales the estimator's variance by approximately  $\Gamma^2 := \prod_{k=1}^K \gamma(\mathbf{C}_k)^2$ , thereby requiring the number of samples to increase by a factor of  $\Gamma^2$  to maintain a fixed estimation error.

### Appendix C: Time-Evolution by Probabilistic Angle Interpolation (TE-PAI)

This section briefly reviews the result on TE-PAI method proposed in Ref. [13], including the asymptotic analysis on expected gate count and variance. TE-PAI method applies probabilistic angle interpolation (PAI) [14] to Pauli rotations gates. The analytic expression of the coefficients in Eq. (3) is explicitly given as follows:

$$\begin{aligned} a_1(\theta) &= \csc\left(\frac{\Delta}{2}\right) \cos\left(\frac{\theta}{2}\right) \sin\left(\frac{\Delta}{2} - \frac{\theta}{2}\right), \\ a_2(\theta) &= \csc(\Delta) \sin(\theta), \\ a_3(\theta) &= -\sec\left(\frac{\Delta}{2}\right) \sin\left(\frac{\theta}{2}\right) \sin\left(\frac{\Delta}{2} - \frac{\theta}{2}\right). \end{aligned} \quad (\text{C1})$$

Since this is quasiprobability decomposition by construction, the following random map is an unbiased estimator of the ideal rotation channel  $\mathbf{R}_{P,\theta}$ :

$$\mathbb{E}[\gamma(\theta) \text{sign}(a_l(\theta)) \mathbf{R}_{P,l}] = \mathbf{R}_{P,\theta},$$

Subsequently, the TE-PAI channel Eq. (4) along with classical weight form an unbiased estimator of the Trotterized time evolution channel as:

$$\mathbb{E}\left[\Gamma_l \hat{\mathbf{U}}_{l,t}^{(K)}\right] = \mathbf{U}_{H,t}^{(K)}.$$

As  $K$  increases, the reduced rotation angles  $\theta_j$  cause the probability of sampling the identity gate to approach one. This mechanism probabilistically skips the majority of operations, yielding a sampled circuit with depth  $\nu_l \ll JK$ , significantly shallower than the original Trotter sequence. As a consequence, the expected number of non-identity gates  $\mathbb{E}[\nu_l]$  scales linearly with  $t$  and converges to constant in the large  $K$  limit,

$$\mathbb{E}[\nu_l] = \csc(\Delta) (3 - \cos \Delta) \|H\|_1 t + O(1/K),$$

whereas the number of gates in Trotter scale as  $O(t^2)$  and diverge as  $K \rightarrow \infty$ . Here  $\|H\|_1 := \sum_j |h_j|$  is the  $L^1$

norm of the Hamiltonian coefficients. This depth reduction comes at the cost of a statistical sampling overhead, captured by the accumulated weight  $\Gamma$ . Here, the overhead factor  $\Gamma^2$  scales exponentially with the evolution time  $t$  as, however, it converges to a constant in the large  $K$  limit:

$$\Gamma^2 = \exp\left[2t\|H\|_1 \tan\left(\frac{\Delta}{2}\right)\right] + O(1/K).$$

The advantage of TE-PAI lies in its tunable parameter  $\Delta$ , which explicitly governs the trade-off between circuit depth and sampling overhead. In the large- $K$  limit, increasing  $\Delta$  reduces the expected circuit depth but increases the sampling overhead; decreasing  $\Delta$  has the opposite effect, lowering the sampling cost at the expense of deeper circuits. As remarked in Ref. [13], by setting  $\Delta$  to a sufficiently small value defined by  $\Delta = 2 \arctan\left(\frac{Q}{2\|H\|_1 t}\right)$ , TE-PAI achieves a constant measurement overhead  $\exp(Q)$  while the gate count scales as  $\mathcal{O}\left(\frac{\|H\|_1^2 t^2}{Q}\right)$ , which is comparable to the standard Trotter approach.

Furthermore, Ref. [13] demonstrated that TE-PAI is highly advantageous for the early-FTQC regime. Since the only non-Clifford operation required is  $R_Z(\Delta)$ , the protocol offers the potential to significantly reduce the number of T-gates needed to execute a single circuit instance.

### Appendix D: Algorithmic shadow spectroscopy

Let  $H$  be an  $N$ -qubit Hamiltonian with eigenstates  $|E_\alpha\rangle$  for  $\alpha = 1, \dots, 2^N$  and corresponding eigenvalues  $E_\alpha$ . To obtain energy differences,  $E_\alpha - E_\beta$ , algorithmic shadow spectroscopy uses expectation values of a set of observables  $\{O_i\}_{i=1}^{N_o}$  consisting of all  $q$ -local Pauli operators, evaluated with respect to time-evolved states  $|\rho(t)\rangle = \mathbf{U}_{H,t}|\rho_{\text{init}}\rangle$  for some initial state  $|\rho_{\text{init}}\rangle$  [9].

The algorithm is as follows. Let  $\{t_n\}_{n=1}^{N_t}$  be a set of time points and define  $S_i(n) := \langle\langle O_i | \rho(t_n) \rangle\rangle$ .

1. Gather shadow snapshots of  $\rho(t_n)$  for each  $t_n$  using  $N_s$  copies of  $\rho(t_n)$ . This is the only step performed on quantum hardware; the following steps are classical.
2. Estimate  $\hat{S}_i(n)$  from the snapshots.
3. Construct a data matrix  $D \in \mathbb{R}^{N_o \times N_t}$  with entries  $D_{i,n} = \frac{\hat{S}_i(n) - \mu_i}{\sigma_i}$  and  $\mu_i, \sigma_i$  are the mean and standard deviation of  $\{\hat{S}_i(n)\}_{n=1}^{N_t}$ , respectively.
4. Apply the Ljung-Box test to each row of  $D$  to remove signals indistinguishable from noise [32, 33].
5. Compute the correlation matrix

$$C = DD^\top \in \mathbb{R}^{N_o \times N_o}, \quad (\text{D1})$$

and extract the top  $c$  dominant eigenvectors  $\{v_1, v_2, \dots, v_c\}$  corresponding to the largest eigenvalues [34].

6. Compute the spectral cross-correlation matrix

$$x_{kl}(m) = \sum_{n=1}^{N_t-m-1} v_k(n+m) v_l(n), \quad (\text{D2})$$

and perform a discrete Fourier transform (DFT) of  $x_{kl}(m)$  with respect to the time lag index  $m$ . Denote the resulting quantity by  $X_{kl}(m)$ , where  $m$  now represents the frequency index.

7. Compute the largest singular value  $\lambda(m)$  of the matrix  $X(m)$ . Peaks in  $\lambda(m)$  correspond to the energy gaps of the Hamiltonian.

## Appendix E: Formal Analysis of the TE-PAI shadow Estimator

Algorithm 2 shows the detailed pseudocode of the practical implementation of our protocol used in the experiments. As discussed in the main text, this implementation is designed to generate one time-evolution circuit via the TE-PAI process and reuses it with  $N_s$  different randomized measurement bases to obtain  $N_s$  snapshots for each TE-PAI sampled circuits. Theorems 1 and 2 establish that this modified implementation yields an unbiased estimator and provides an explicit upper bound on the variance.

Before proving Theorems 1 and 2, we first present a lemma that upper bounds the variance of an expectation value for a single quasiprobability random circuit.

**Lemma 1.** *The expectation value of any observable  $O$  under a quasiprobability random circuit yields an unbiased estimator of the true expectation value:*

$$\mathbb{E}[\Gamma_l \langle\langle O | \hat{C}_l(\rho) \rangle\rangle] = \langle\langle O | \mathbf{C}(\rho) \rangle\rangle.$$

Additionally, the variance is upper bounded as follows:

$$\text{Var} \left[ \Gamma_l \langle\langle O | \hat{C}_l(\rho) \rangle\rangle \right] \leq \Gamma^2 \|O\|^2.$$

*Proof.* The unbiasedness directly follows from the unbiasedness of the TE-PAI decomposition:

$$\begin{aligned} \mathbb{E}[\Gamma_l \langle\langle O | \hat{C}_l(\rho) \rangle\rangle] &= \langle\langle O | \mathbb{E}[\Gamma_l \hat{C}_l](\rho) \rangle\rangle \\ &= \langle\langle O | \mathbf{C}(\rho) \rangle\rangle \end{aligned}$$

Write  $\hat{o} := \Gamma_l \langle\langle O | \hat{C}_l(\rho) \rangle\rangle$  for brevity. The variance is given by  $\text{Var}[\hat{o}] = \mathbb{E}[\hat{o}^2] - \mathbb{E}[\hat{o}]^2 = \mathbb{E}[\hat{o}^2] - \langle\langle O | \mathbf{C}(\rho) \rangle\rangle^2$ , and we now upper bound the first term as

$$\begin{aligned} \mathbb{E}[\hat{o}^2] &= \sum_l p_l \times [\Gamma_l \langle\langle O | \mathbf{C}_l(\rho) \rangle\rangle]^2 \\ &= \Gamma^2 \sum_l p_l \times \langle\langle O | \mathbf{C}_l(\rho) \rangle\rangle^2 \\ &\leq \Gamma^2 \|O\|^2 \end{aligned}$$

Above we have used that  $|\langle\langle O | \rho \rangle\rangle| \leq \|O\|$  for any density matrix  $\rho$  and  $\sum_l p_l = 1$ .  $\square$

### 1. Proof of Theorem 1

This modified implementation preserves the unbiased nature of the estimator.

*Proof.* The goal is to estimate the true expectation value of an observable  $O$ , defined with respect to the original channel  $\langle\langle O | \mathbf{C}(\rho) \rangle\rangle$ . Our final estimator,  $\langle\langle \hat{O} \rangle\rangle$ , is the average over all measurement outcomes. More specifically, let  $o_{m,s}$  be the outcome from the  $m$ -th quasiprobability random circuit and the  $s$ -th shadow snapshot, that is,

$$o_{m,s} = \Gamma_{l_m} \langle\langle O | \hat{\rho}_{m,s} \rangle\rangle,$$

where  $\Gamma_{l_m}$  is the weight accumulated from the  $m$ -th quasiprobability sample and  $\hat{\rho}_{m,s}$  is the corresponding classical shadow snapshot defined in (6). The estimator is constructed as

$$\langle\langle \hat{O} \rangle\rangle = \frac{1}{MN_s} \sum_{m=1}^M \sum_{s=1}^{N_s} o_{m,s}.$$

The expectation value of this estimator,  $\mathbb{E}[\langle\langle \hat{O} \rangle\rangle]$ , is taken over both the probabilistic choice of  $\Gamma_{l_m}$  and the shadow's random choice of measurement bases. We can analyze the expectation in steps, from the inside out using the *law of total expectation*. First, the inner expectation is a conditional expectation over the shadow measurement outcomes, given a fixed quasiprobability random circuit  $\mathbf{C}_{l_m}$ . We denote this expectation by  $\mathbb{E}_{\text{sh}}$  and we have

$$\begin{aligned} \mathbb{E}_{\text{sh}} \left[ \frac{1}{N_s} \sum_{s=1}^{N_s} o_{m,s} \right] &= \frac{1}{N_s} \sum_{s=1}^{N_s} \mathbb{E}_{\text{sh}} [o_{m,s}] \\ &= \langle\langle O | \Gamma_{l_m} \mathbf{C}_{l_m}(\rho) \rangle\rangle. \end{aligned} \quad (\text{E1})$$

Next, we consider the outer average over the  $M$  samples. The Quasiprobability sampling protocol is constructed to be an unbiased estimator of the exact time-evolution channel, meaning  $\mathbb{E}_{\Gamma_l} [\Gamma_{l_m} \mathbf{C}_{l_m}] = \mathbf{C}$ . By the linearity of expectation and trace, the full expectation value is

$$\begin{aligned} \mathbb{E}[\langle\langle \hat{O} \rangle\rangle] &= \mathbb{E}_{\Gamma_l} \left[ \frac{1}{M} \sum_{m=1}^M \mathbb{E}_{\text{sh}} \left[ \frac{1}{N_s} \sum_{s=1}^{N_s} o_{m,s} \right] \right] \\ &= \frac{1}{M} \sum_{m=1}^M \mathbb{E}_{\Gamma_l} [\langle\langle O | \Gamma_{l_m} \mathbf{C}_{l_m}(\rho) \rangle\rangle] \\ &= \langle\langle O | \mathbb{E}_{\Gamma_l} [\Gamma_{l_m} \mathbf{C}_{l_m}](\rho) \rangle\rangle \\ &= \langle\langle O | \mathbf{C}(\rho) \rangle\rangle \end{aligned}$$

$\square$

## 2. Proof of Theorem 2

*Proof.* Let  $Y_m$  denote the estimator obtained from the  $m$ -th sampled circuit, averaged over its  $N_s$  shadow snapshots:

$$Y_m = \frac{1}{N_s} \sum_{s=1}^{N_s} o_{m,s}.$$

Since the  $M$  circuit samples are independent and identically distributed, the total variance is  $\text{Var}[\langle \hat{O} \rangle] = \frac{1}{M} \text{Var}[Y_m]$ . We apply the Law of Total Variance to  $Y_m$ , conditioning on the choice of the random circuit  $\mathcal{C}_{l_m}$ . Let  $\mathbb{E}_l$  and  $\text{Var}_l$  denote the expectation and variance over the circuit distribution given by the quasiprobability sampling, and  $\mathbb{E}_{\text{sh}}$  and  $\text{Var}_{\text{sh}}$  denote the conditional expectation and variance over the shadow measurement randomness, given a fixed random circuit  $\mathcal{C}_{l_m}$ . The total variance decomposes as

$$\text{Var}[Y_m] = \text{Var}_l(\mathbb{E}_{\text{sh}}[Y_m]) + \mathbb{E}_l[\text{Var}_{\text{sh}}(Y_m)].$$

Conditioned on a specific circuit  $\mathcal{C}_m$ , the shadow estimator is unbiased for that circuit's observable value as Eq. (E1). From Lemma 1, the first term is upper bounded as

$$\text{Var}_l(\mathbb{E}_{\text{sh}}[Y_m]) \leq \Gamma^2 \|O\|^2 - \langle\langle O | \mathcal{C}(\rho) \rangle\rangle^2. \quad (\text{E2})$$

Conditioned on a fixed random circuit  $\mathcal{C}_{l_m}$ ,  $Y_m$  is the average of  $N_s$  independent snapshots. The variance of a single weighted snapshot  $\Gamma_m \text{Tr}(O\hat{\rho})$  is determined by the second moment of the shadow estimator as  $\mathbb{E}_{\text{sh}}[\langle\langle O | \hat{\rho} \rangle\rangle^2] \leq \|O\|_{\text{sh}}^2$ . Thus, the variance of a single snapshot given  $\mathcal{C}_m$  is:

$$\text{Var}_{\text{sh}}(\Gamma_{l_m} \langle\langle O | \hat{\rho}_{m,s} \rangle\rangle) \leq \Gamma^2 (\|O\|_{\text{sh}}^2 - \langle\langle O | \mathcal{C}_{l_m}(\rho) \rangle\rangle^2).$$

Since  $Y_m$  averages  $N_s$  such snapshots, its conditional variance is scaled by  $1/N_s$ :

$$\text{Var}_{\text{sh}}(Y_m) = \frac{\Gamma^2}{N_s} (\|O\|_{\text{sh}}^2 - \langle\langle O | \mathcal{C}_{l_m}(\rho) \rangle\rangle^2).$$

Taking the expectation over circuits yields the second term of the total variance:

$$\begin{aligned} \mathbb{E}_l[\text{Var}_{\text{sh}}(Y_m)] &= \frac{\Gamma^2}{N_s} \left( \|O\|_{\text{sh}}^2 - \mathbb{E}_l[\langle\langle O | \mathcal{C}_{l_m}(\rho) \rangle\rangle^2] \right) \\ &\leq \frac{\Gamma^2}{N_s} (\|O\|_{\text{sh}}^2 - \|O\|^2). \end{aligned} \quad (\text{E3})$$

Summing Eq. (E2) and Eq. (E3) gives  $\text{Var}[Y_m]$ :

$$\text{Var}[Y_m] \leq \frac{\Gamma^2}{N_s} \|O\|_{\text{sh}}^2 + \left( 1 - \frac{1}{N_s} \right) \Gamma^2 \|O\|^2.$$

Finally, dividing by  $M$  yields the variance of the total estimator  $\langle \hat{O} \rangle$ :

$$\text{Var}[\langle \hat{O} \rangle] \leq \Gamma^2 \left( \frac{\|O\|_{\text{sh}}^2 - \|O\|^2}{MN_s} + \frac{\|O\|^2}{M} \right).$$

□

---

### Algorithm 2 Experimental implementation of shadow snapshots

---

**Input:** Hamiltonian  $H$ , initial state  $\rho_{\text{init}}$ , total time  $t$ , Trotter steps  $K_{\text{steps}}$ , angle  $\Delta$ , number of TE-PAI samples  $M_{\text{TE-PAI}}$ , number of shadow snapshots per sample  $N_s$   
**Output:** A collection of  $N = M_{\text{TE-PAI}} \times N_s$  shadow snapshot tuples  $(\Gamma, \{U_n\}_{n=1}^N, \{b_n\}_{n=1}^N)$

```

1: Initialize an empty list of snapshots  $\mathcal{S}$ 
2: for  $m = 1$  to  $M_{\text{TE-PAI}}$  do
3:   Initialize TE-PAI weight  $\Gamma_m \leftarrow 1$ 
4:   Initialize an empty quantum circuit for evolution  $\mathcal{C}_{\text{evol}}$ 
5:   Set  $\delta = t/K_{\text{steps}}$ 
6:   for  $k = 1$  to  $K_{\text{steps}}$  do
7:     for  $j = 1$  to  $J$  do
8:       Compute  $\theta_j = 2h_j\delta$  and coefficients  $a_1, a_2, a_3$ 
9:       Set  $\gamma = |a_1| + |a_2| + |a_3|$ .
10:      Sample  $d$  with probability  $|a_d|/\gamma$ 
11:      Update  $\Gamma_m \leftarrow \Gamma_m \times \gamma \times \text{sign}(a_d)$ 
12:      Append the corresponding gate to  $\mathcal{C}_{\text{evol}}$ 
13:    end for
14:  end for
15:  for  $s = 1$  to  $N_s$  do
16:    Create a copy:  $\mathcal{C}_{\text{total}} \leftarrow \mathcal{C}_{\text{evol}}$ 
17:    for  $n = 1$  to  $N$  do
18:      Sample a Clifford gate  $U_n$  uniformly at random
19:      Append  $U_n$  to qubit  $n$  in  $\mathcal{C}_{\text{total}}$ 
20:    end for
21:    Apply  $\mathcal{C}_{\text{total}}$  to  $\rho_{\text{init}}$  and measure to get bitstring  $b$ 
22:    Append the tuple  $(\Gamma_m, \{U_n\}, b)$  to  $\mathcal{S}$ 
23:  end for
24: end for
25: return  $\mathcal{S}$ 

```

---

## Appendix F: Energy Spectrum of the Heisenberg Hamiltonian

In condensed matter physics, the isotropic Heisenberg model is typically defined using spin-1/2 operators  $\mathbf{S}_i = \frac{1}{2}\boldsymbol{\sigma}_i$ , where  $\boldsymbol{\sigma} = (X, Y, Z)$  are the Pauli matrices [35, 36]. The standard Hamiltonian is:

$$\mathcal{H} = J \sum_{i=1}^{N-1} (\mathbf{S}_i \cdot \mathbf{S}_{i+1} + 1). \quad (\text{F1})$$

Our simulation employs Pauli operators directly, implying a scaling of  $\boldsymbol{\sigma}_i \cdot \boldsymbol{\sigma}_{i+1} = 4(\mathbf{S}_i \cdot \mathbf{S}_{i+1})$ . Consequently, all eigenvalues are scaled by a factor of 4 relative to the classic Bethe Ansatz results [37]. For an infinite chain, the ground state energy  $E_0$  follows the Hulthén integral [38], while low-lying excitations are described by des Cloizeaux-Pearson magnon triplets [39]. In our finite  $N = 10$  system with open boundary conditions and  $J = 1$ , exact diagonalization reveals a discrete spectrum governed by  $SU(2)$  symmetry. The ground state and the 10th energy level, which resides in the third excited manifold, yield the following numerical results:  $E_{\text{Groundstate}} = -17.0321$  and  $E_{10^{\text{th}}} = -12.6726$  resulting theoretical energy gap for our state preparation :

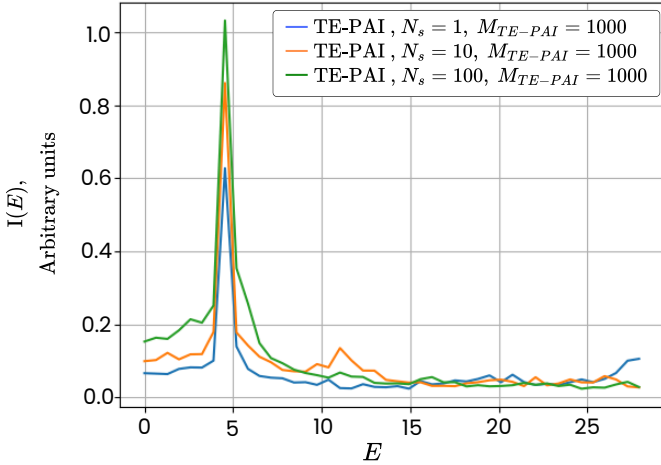


FIG. 4. Comparison of TE-PAI spectra computed with different shadow sizes. The spectra were generated using a fixed number of TE-PAI samples while varying the shadow size  $N_s \in \{1, 10, 100\}$ , respectively blue, orange and green spectrum. While all cases resolve the theoretical energy gap, increasing  $N_s$  significantly enhances the peak intensity. Simulation parameters match those detailed in Sec. IV A.

$\Delta E \approx 4.3595$ . This gap represents the energy required to sustain multi-magnon excitations within the quantized momentum space of a 10-qubit chain.

#### Appendix G: Influence of the Shadow size on the TE-PAI spectrum

We now examine how shadow size influences the resulting spectrum. Fig. 4 presents three TE-PAI spectra obtained using a fixed number of TE-PAI samples across varying shadow sizes,  $N_s \in \{1, 10, 100\}$ . All simulations utilized the parameters defined in Sec. IV A. While all three spectra successfully resolve the theoretical energy gap, the peak intensity increases significantly with larger shadow sizes. However, a larger shadow size imposes a substantial computational overhead, as the total number of circuit executions scales with  $M_{TE-PAI} \times N_s$ . In the study we fix the shadow size to  $N_s = 1$  and only change the number of TE-PAI sample.

#### Appendix H: Hardware properties

Table I summarizes the hardware characteristics of the two IBM Quantum backends used in this study: *ibm\_kobe* and *ibm\_kingston*. Both devices are based on the Heron r2 architecture and provide identical native basis gate sets, consisting of `cz`, `id`, `rx`, `rz`, `rzz`, `sx`, and `x`. This extensive gate set allows for greater flexibility in circuit design, particularly by enabling simulation of more complex Hamiltonians natively, without requiring excessive transpilation. Despite architectural similarities, the

TABLE I. Comparison of processor performance metrics between *ibm\_kobe* and *ibm\_kingston*.

Processor	<i>ibm_kobe</i>	<i>ibm_kingston</i>
2Q error (best)	$1.03 \times 10^{-3}$	$1.06 \times 10^{-3}$
2Q error (layered)	$2.68 \times 10^{-3}$	$3.64 \times 10^{-3}$
CLOPS	$2.5 \times 10^5$	$2.5 \times 10^5$
Median CZ error	$1.858 \times 10^{-3}$	$2.088 \times 10^{-3}$
Median SX error	$2.383 \times 10^{-4}$	$2.379 \times 10^{-4}$

backends differ slightly in their two-qubit gate fidelity. *ibm\_kobe* exhibits a lower two-qubit gate error, both in the best-case scenario ( $1.03 \times 10^{-3}$ ) and in layered execution ( $2.68 \times 10^{-3}$ ), compared to *ibm\_kingston*, which shows  $1.06 \times 10^{-3}$  and  $3.64 \times 10^{-3}$ , respectively. This improved fidelity makes *ibm\_kobe* a better candidate for experiments requiring two qubit gates. Although the differences in fidelity are marginal, *ibm\_kobe*'s slightly better two-qubit performance and its alignment with low transpilation depth makes it our preferred choice for hardware-based simulations involving entanglement-heavy operations.

The logical-to-physical mapping is performed based on an optimization strategy prioritizing long  $T_1/T_2$  and low error rates.

Figure 5 and Figure 6 show diagram of the physical mapping of qubits.

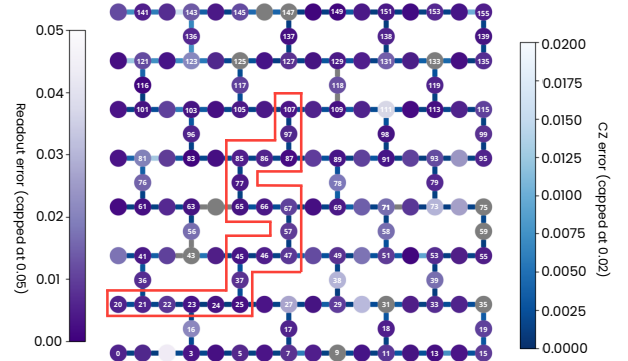


FIG. 5. Architecture and error landscape of the *ibm\_kobe* quantum processor. Each node represents a qubit, with its color indicating the average readout assignment error. Each edge represents a physical connection between two qubits, and its color encodes the average controlled-Z (CZ) gate error. Grey nodes or edges indicate that the corresponding error exceeds a predefined threshold, set to 0.05 for the readout error and 0.02 for the CZ error. The qubits and connections highlighted by the red outline denote the specific subset of the device that is utilized in our experiments.

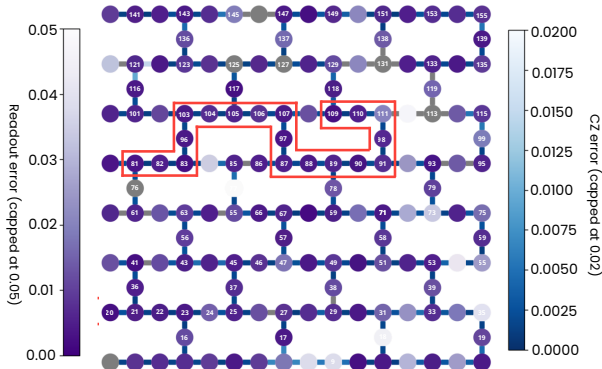


FIG. 6. Same as Fig. 5, but for the *ibm-kingston* quantum processor.

- [1] S. Sachdev, *Quantum Phase Transitions*, 2nd ed. (Cambridge University Press, 2011).
- [2] I. N. Levine, *Quantum Chemistry*, 6th ed. (Pearson Prentice Hall, London, 2009).
- [3] P. A. M. Dirac, Quantum mechanics of many-electron systems, *Proceedings of the Royal Society of London. Series A* **123**, 714 (1929).
- [4] S. Lloyd, Universal quantum simulators, *Science* **273**, 1073 (1996).
- [5] Z. Zimborás, B. Koczor, Z. Holmes, E.-M. Borrelli, A. Gilyén, H.-Y. Huang, Z. Cai, A. Acín, L. Aolita, L. Banchi, *et al.*, Myths around quantum computation before full fault tolerance: What no-go theorems rule out and what they don't, arXiv preprint arXiv:2501.05694 (2025).
- [6] R. Babbush, R. King, S. Boixo, W. Huggins, T. Khattar, G. H. Low, J. R. McClean, T. O'Brien, and N. C. Rubin, The grand challenge of quantum applications, arXiv preprint arXiv:2511.09124 (2025).
- [7] A. Y. Kitaev, Quantum measurements and the abelian stabilizer problem, arXiv:quant-ph/9511026 [quant-ph] (1995).
- [8] M. A. Nielsen and I. L. Chuang, *Quantum Computation and Quantum Information: 10th Anniversary Edition*, 10th ed. (Cambridge University Press, Cambridge, UK, 2010) p. 702.
- [9] H. H. S. Chan, R. Meister, M. L. Goh, and B. Koczor, Algorithmic shadow spectroscopy, *PRX Quantum* **6**, 010352 (2025).
- [10] H.-Y. Huang, R. Kueng, and J. Preskill, Predicting many properties of a quantum system from very few measurements, arXiv:2002.08953 [quant-ph] (2020).
- [11] H. Jnane, J. Steinberg, Z. Cai, H. C. Nguyen, and B. Koczor, Quantum error mitigated classical shadows, *PRX Quantum* **5**, 010324 (2024).
- [12] S. Endo, S. C. Benjamin, and Y. Li, Practical quantum error mitigation for near-future applications, *Physical Review X* **8**, 031027 (2018).
- [13] C. Kiumi and B. Koczor, Te-pai: Exact time evolution by sampling random circuits (2024), arXiv:2410.16850 [quant-ph].
- [14] B. Koczor, J. J. L. Morton, and S. C. Benjamin, Probabilistic interpolation of quantum rotation angles, *Physical Review Letters* **132**, 130602 (2024).
- [15] B. Koczor, Sparse probabilistic synthesis of quantum operations, *PRX Quantum* **5**, 040352 (2024).
- [16] Y. Kim, A. Eddins, S. Anand, K. Takagi, A. Sharma, E. Van Den Berg, A. Kandala, and K. Temme, Evidence for the utility of quantum computing before fault tolerance, *Nature* **618**, 500 (2023).
- [17] A. Gilchrist, N. K. Langford, and M. A. Nielsen, Distance measures to compare real and ideal quantum processes, *Physical Review A* **71**, 062310 (2005).
- [18] M. Suzuki, Fractal decomposition of exponential operators with applications to many-body theories and monte carlo simulations, *Physics Letters A* **146**, 319 (1990).
- [19] M. Suzuki, General theory of fractal path integrals with applications to many-body theories and statistical physics, *Journal of Mathematical Physics* **32**, 400 (1991).
- [20] K. Temme, S. Bravyi, and J. M. Gambetta, Error mitigation for short-depth quantum circuits, *Physical Review Letters* **119**, 180509 (2017).
- [21] S. Endo, S. C. Benjamin, and Y. Li, Practical quantum error mitigation for near-future applications, *Physical Review X* **8**, 031027 (2018).
- [22] R. J. Baxter, *Exactly solved models in statistical mechanics* (Academic Press, 1982).
- [23] Qiskit contributors, *Qiskit sdk api reference: QuantumCircuit.depth* (2025), accessed: 2026-01-15.
- [24] P. Pfeuty, The one-dimensional Ising model with a transverse field, *Annals of Physics* **57**, 79 (1970).
- [25] A. M. Childs, Y. Su, M. C. Tran, N. Wiebe, and S. Zhu, Theory of trotter error with commutator scaling, *Physical Review X* **11**, 10.1103/physrevx.11.011020 (2021).
- [26] K. Temme, S. Bravyi, and J. M. Gambetta, Error mitigation for short-depth quantum circuits, *Physical Review Letters* **119**, 180509 (2017).
- [27] H. Jnane, J. Steinberg, Z. Cai, H. C. Nguyen, and B. Koczor, Quantum error mitigated classical shadows, *PRX Quantum* **5**, 010324 (2024).

[28] B. Koczor, J. J. L. Morton, and S. C. Benjamin, Probabilistic interpolation of quantum rotation angles, *Physical Review Letters* **132**, 10.1103/physrevlett.132.130602 (2024).

[29] T. Peng, A. W. Harrow, M. Ozols, and X. Wu, Simulating large quantum circuits on a small quantum computer, *Phys. Rev. Lett.* **125**, 150504 (2020).

[30] K. Mitarai and K. Fujii, Constructing a virtual two-qubit gate by sampling single-qubit operations, *New J. Phys.* **23**, 023021 (2021), (arXiv:1909.07534).

[31] A. W. Harrow and A. Lowe, Optimal quantum circuit cuts with application to clustered hamiltonian simulation, *PRX Quantum* **6**, 010316 (2025).

[32] G. E. P. Box and D. A. Pierce, Distribution of residual autocorrelations in autoregressive-integrated moving average time series models, *Journal of the American Statistical Association* **65**, 1509 (1970).

[33] G. M. LJUNG and G. E. P. BOX, On a measure of lack of fit in time series models, *Biometrika* **65**, 297 (1978).

[34] R. Bronson and G. B. Costa, Chapter 6 - eigenvalues and eigenvectors, in *Matrix Methods (Fourth Edition)*, edited by R. Bronson and G. B. Costa (Academic Press, 2021) fourth edition ed., pp. 185–223.

[35] M. Takahashi, *Thermodynamics of One-Dimensional Solvable Models* (Cambridge University Press, 1999).

[36] D. C. Mattis, *The Theory of Magnetism I: Statics and Dynamics* (Springer-Verlag, 1981).

[37] H. Bethe, Zur theorie der metalle, *Zeitschrift für Physik* **71**, 205 (1931).

[38] L. Hulthén, Über das austauschproblem eines kristalls, *Arkiv für Matematik, Astronomi och Fysik* **26A**, 1 (1938).

[39] J. des Cloizeaux and J. J. Pearson, Antiferromagnetic linear chain of spin 1/2, *Physical Review* **128**, 2131 (1962).